Measurement of the Self-Phase Modulation on OMEGA

Introduction

The safe operation of a multikilojoule-class laser system requires that the accumulated nonlinear phase remain low enough to avoid beam filamentation and resulting damage to the laser-amplifier glass. A rule of thumb for infrared lasers is to keep the so-called ΔB-integral below 2 radians,[1] where the B-integral is given by

$$B(t) = \frac{2\pi}{\lambda} \int_0^L \gamma(z) \times I(z,t) \times \mathrm{d}z \qquad (1)$$

for a wavelength λ, optical path length L, nonlinear coefficient γ, and intensity $I(z,t)$, which equals the power divided by the area $P(z,t)/A(z)$. While ΔB, which is calculated per stage, where a stage is defined as all of the components between sequential spatial filters, is of most interest, a potentially more easily measured quantity is the ΣB of the system or the sum of B-integral through all stages of the system.[2] The protocols for safe operation become particularly important on a system like LLE's OMEGA laser. The OMEGA Laser System consists of 60 beamlines with nine amplification stages employing Nd:phosphate glass (LHG8). Each beamline typically produces about 800 J of infrared energy (λ_{IR} = 1053 nm) in a 1-ns super-Gaussian pulse. This energy is converted to the UV (λ_{UV} = 351 nm) by frequency tripling in KDP crystals with approximately 60% conversion efficiency. The temporal pulse shape is adjusted from shot to shot as specified by the principal investigator. Some of these pulse shapes have rapid changes in intensity that can increase the self-phase modulation (SPM) beyond acceptable limits.

Before any of these pulse shapes is propagated down the system, a computer code that incorporates the Frantz–Nodvik model of light propagation in a laser amplifier chain[3] simulates the pulse through the system. These simulations have been extensively tested with respect to the temporal pulse shape. The code also predicts the SPM experienced by the pulse due to the B-integral. By introducing an imaging spectrometer at the output of the laser system, it is possible for the first time to directly compare the model's prediction of the ΣB-integral with a shift in the laser frequency.

The change in instantaneous frequency, $\Delta\nu$, of the pulse caused by SPM is given by[4]

$$\Delta\nu(t) = -\frac{1}{2\pi}\frac{\mathrm{d}B(t)}{\mathrm{d}t} = -\frac{1}{\lambda}\int_0^L \frac{\gamma(z)}{A(z)} \times \frac{\mathrm{d}P(z,t)}{\mathrm{d}t} \times \mathrm{d}z. \qquad (2)$$

Therefore, the instantaneous change in the optical frequency is proportional to the time derivative of the B-integral. If the temporal pulse shape is assumed to be independent of z, the derivative of intensity can be removed from the integrand in Eq. (2) and the instantaneous frequency is simply proportional to $\mathrm{d}P/\mathrm{d}t$. This assumption is not valid in most laser amplifier systems. Typically a low-energy pulse injected at the front end of the system is continuously amplified as it propagates. On OMEGA, a single laser pulse feeds all 60 beamlines. The intensity increases as the beam passes through an amplifier stage and then decreases as the beam is split to feed subsequent amplifier stages. The pulse shape, injected at the input of the system, is typically a monotonically increasing temporal ramp. The leading edge of this ramp is preferentially amplified relative to the trailing edge because of the gain–saturation dynamics of the glass amplifiers. Depending on the exact shape of the input pulse, the output pulse shape can be a rising ramp, a super-Gaussian flattop, or a falling ramp. For the purposes of this article, only Gaussian and flattop pulses will be considered. The correct way to handle all these pulse shapes is to calculate $\Delta\nu(z)$ at every point in the laser-amplifier chain and produce an integrated frequency shift for the entire system. This ability is incorporated in the laser system model mentioned above.

Based on temporal and spatial measurements that can be made on the system, we have verified the predictions of the model both in terms of pulse shape and ΣB-integral. Additionally, we have demonstrated that $\Delta\nu$ is approximately proportional to $\mathrm{d}P/\mathrm{d}t$ as measured in the UV at the output of the laser chain. This relationship is the basis of an empirical analysis

that assumes that the intensity is independent of z. Although this empirical analysis is less accurate than the full-system model, it has the advantage of being available immediately after a shot has been taken, as opposed to more than 1 h for a full simulation. Therefore, this relationship provides a real-time diagnostic that can immediately determine if the laser system is being operated safely. The agreement between the empirical model and the measurements is sufficient for a "go/no-go" decision in terms of shot operations.

The primary modeling tool used here—the *RAINBOW* code—calculates energy transport in solid-state laser systems and uses ray tracing to propagate a pulse through all components of a laser chain. Laser amplifiers are modeled by numerically solving the Frantz–Nodvik[3] equations as modified by Avizonis and Grotbeck[5] on a time-resolved basis for one or more locations in the aperture of the laser. Arbitrary spatial and temporal pulse shapes may be input, allowing for detailed predictions of the spatial and temporal shapes of the laser output. Gain saturation is modeled using a variant of the two-ion model[6] derived from fits to gain-saturation data.[7] Disk- and rod-geometry gain elements are modeled. Passive losses are input for each component. Frequency conversion to the third harmonic uses intensity look-up tables from *MIXER* code[8] calculations.

RAINBOW accurately tracks the accumulated phase retardation of each temporal element of each ray (the "B" integral) and includes a phenomenological model of spatial-filter transmission.[9] Using the determined SPM, it calculates the output pulse spectrum by a Fourier transformation.

Measurement

The temporal pulse shape is measured at both the input and output of the system. After an initial temporal pulse–shaping system, the infrared pulse shape is measured with either an 18-GHz InGaAs photodiode[10] or a streak camera with an S-1 photocathode. The IR measurements are used as the input to the model. At the output of the system, the intensity as a function of time is measured for each of the 60 beamlines on OMEGA with a set of six streak cameras that have a 50-ps temporal resolution.[11] Figure 124.16 shows a measured IR pulse shape at the input of the system (scaled to match the peak UV power), a predicted UV pulse shape at the end of the system, and a measured UV output pulse. The excellent agreement between the model and the measurement provides an experimental verification of the model. In addition, an imaging spectrometer measures the UV spectra of all 60 beams with a 2.5-pm (7.6-GHz) resolution.[12] These two sets of measurements can be combined to demonstrate a linear relationship between dP/dt and the frequency shift caused by SPM.

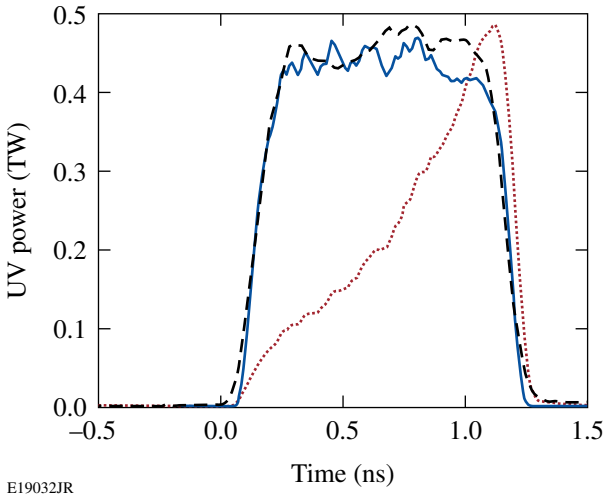

Figure 124.16
The temporal UV pulse shape at the output of the system as measured by the streak cameras (dashed black curve) matches the predicted pulse shape (solid blue curve) derived from the rescaled input IR pulse (dotted red curve).

When relatively benign pulse shapes are propagated on the OMEGA Laser System, such as a 200-J, 2-ns square pulse, only negligible amounts of additional bandwidth are generated. Any observed broadening represents the instrument response function of the spectrometer with a full width, $\Delta\nu$, at 1/20th of the peak of 20 GHz. In contrast, the most-pronounced frequency shifts occur when the amplifier chains generate 40 J of UV energy in a 100-ps FWHM asymmetric Gaussian pulse given approximately by

$$P(t) = P_0 \times e^{-\left[(t-t_0)/\tau\right]^2}, \tag{3}$$

where τ = 49 ps if $t < t_0$ and τ = 80 ps if $t \geq t_0$. In this case dP/dt is non-negligible (>1 GW/ps) for most of the duration of the pulse, so most of the energy is shifted out of the narrow bandwidth defined by the instrument response function. Figure 124.17 shows the spectra from three different laser shots. The dashed green curve from a 63-J, 3-ns square pulse essentially represents the instrument-response function. The solid blue curve, from the 100-ps pulse described above, shows significant spectral broadening.

Similar shifts occur with 1-ns square pulses that rise to the same intensity as the 100-ps pulses with approximately the same rise time. For the 1-ns square pulses, however, most of the pulse energy remains within a narrow spectral bandwidth defined by a monochromatic seed laser because dP/dt

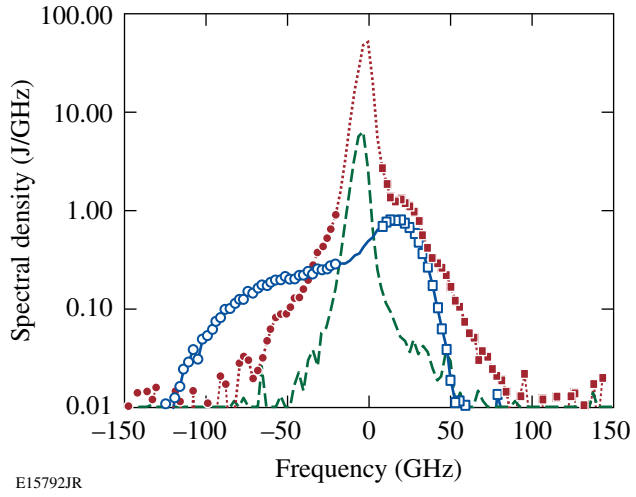

Figure 124.17
The UV spectrum at the output of the system for a 1-ns, 556-J square pulse (dotted red curve), a 100-ps, 48-J pulse (solid blue curve), and a 3-ns, 63-J square pulse (dashed green curve). The squares represent spectral components that have been frequency upshifted; the circles and dots have been downshifted. The 3-ns pulse does not undergo SPM.

is approximately zero (<1 GW/ps) over much of the pulse. The 100-ps pulses produce frequencies that are shifted by as much as 50 GHz from the laser carrier frequency. The integrated effective red and blue spectral shifts for each beamline can be determined from the spectral measurements. From Eq. (2), it can be shown that the rising edge of a pulse ($dP/dt > 0$) gives rise to a red shift ($\Delta\nu < 0$) and the falling edge ($dP/dt < 0$) generates a blue shift ($\Delta\nu > 0$). An effective $\langle dP/dt\rangle$ for the rising edge of the UV pulse is determined by computing a normalized, weighted integral of the time derivative of the power from the 10% to the 80% points on the rising edge:

$$\left\langle \frac{dP_{UV}}{dt} \right\rangle_{rise} = \int_{0.1\,P_{max}}^{0.8\,P_{max}} \frac{dP_{UV}(t)}{dt} \times P_{UV} \times dt \Bigg/ \int_{0.1\,P_{max}}^{0.8\,P_{max}} P_{UV} \times dt. \quad (4)$$

A similar equation can be generated for the falling edge.

Just as the temporal pulse shape can be divided into rising and falling edges, the UV spectra can be divided into red and blue components by determining where energy has been shifted to lower or higher frequencies. To calculate the frequency-shifted spectra, the instrument response function was scaled to represent the same energy as was measured for each beamline. The scaled waveform $S_{resp}(\nu)$ was subtracted from the measured waveform $S_{meas}(\nu)$:

$$S_{\Delta}(\nu) = \left[S_{meas}(\nu) - S_{resp}(\nu)\right]. \quad (5)$$

Anywhere the result is positive represents frequency-shifted energy. Negative numbers represent energy that remained at the center-line frequency of the laser, ν_0. An average, downshifted frequency $\langle\nu_-\rangle$ is defined in a manner similar to $\langle dP/dt\rangle_{rise}$:

$$\langle\nu_-\rangle = \int_{-\infty}^{\nu_0} \nu \times S'_{\Delta}(\nu) \times d\nu \Bigg/ \int_{-\infty}^{\nu_0} S'_{\Delta}(\nu) \times d\nu\,, \quad (6)$$

where $S'_{\Delta} = S_{\Delta}$, if $S_{\Delta} > 0$, and $S'_{\Delta} = 0$, if $S_{\Delta} < 0$. In analogy with the temporal pulse shape, an average upshifted frequency $\langle\nu_+\rangle$ can be similarly defined. The spectral and temporal measurements were combined by pairing $\langle dP/dt\rangle_{rise}$ with $\langle\nu_-\rangle$ and $\langle dP/dt\rangle_{fall}$ with $\langle\nu_+\rangle$. This pairing follows the premise that the rising edge generates red shifts and the falling edge generates blue shifts. When the spectral shifts, recorded for both 1-ns and 100-ps pulses, are plotted versus $\langle dP/dt\rangle$, we find a linear relationship with a slope of –7.8 GHz-ns/TW as shown in Fig. 124.18. As expected, the intercept is approximately zero, which indicates that there is no frequency shift when the intensity is constant. If the amplifier system was characterized by constant power, area, and uniform optical material properties, the slope of the fit in Fig. 124.18 would be directly proportional

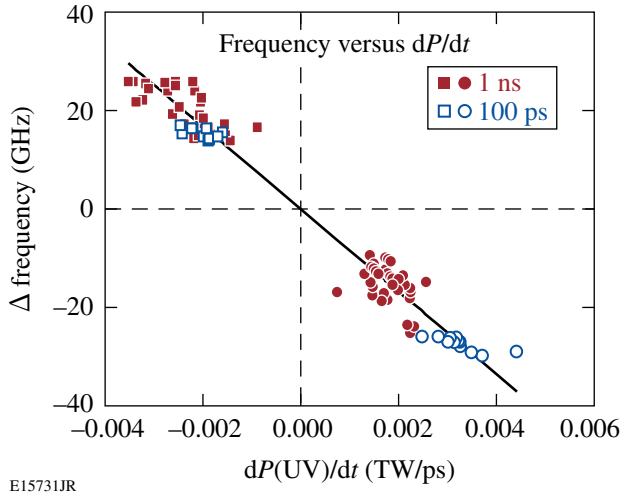

Figure 124.18
Combined plot of $\langle\nu_-\rangle$ versus $\left\langle dP_{rise}/dt\right\rangle$ and $\langle\nu_+\rangle$ versus $\left\langle dP_{fall}/dt\right\rangle$. Data were acquired for both 100-ps double-Gaussian pulses and 1-ns super-Gaussian pulses.

to the nonlinear coefficient of the material, γ. The evolving temporal pulse shape in the amplifier chain implies, however, that the slope represents an effective aggregate value. The fact that there is a linear relationship that extends over different pulse shapes, beamlines, and beam energies is indicative of the reproducibility of the laser system configuration. The utility of the slope lies in the reconstruction of the spectrum from the temporal pulse shape and the extraction of the ΣB-integral from the measured spectrum.

The slope relates the average frequency shift to the average dP/dt. If the relation holds in detail, the same slope relates the instantaneous frequency to the instantaneous dP/dt. The quantity dP/dt was therefore calculated for every time interval dt in the temporal waveform and mapped, via the fitted slope, to a frequency shift. For the simulated curve, dP/dt was derived from the UV power calculated at the end of the amplifier chain by the system model based on the measured IR input pulse. The energy associated with that frequency shift is given by $P(t)dt$. For comparison with the measured spectrum, this energy is distributed over all frequencies using the instrument response function centered at the instantaneous frequency. Finally, the full spectrum is computed by summing the contributions of all time intervals. The result (Fig. 124.19) shows a comparison of the calculated spectra using this technique as derived from the temporal pulse shape (red curve with diamonds) with the directly measured spectra (black curve with ×'s) and the spectrum predicted for the full-system model (solid blue curve). In all three curves, the frequency components with spectral shifts less than ±6 GHz, corresponding to the spectrometer resolution, have been removed to highlight the SPM-induced frequencies. The agreement is remarkably good despite violating the assumption about the constancy of the intensity throughout the system.

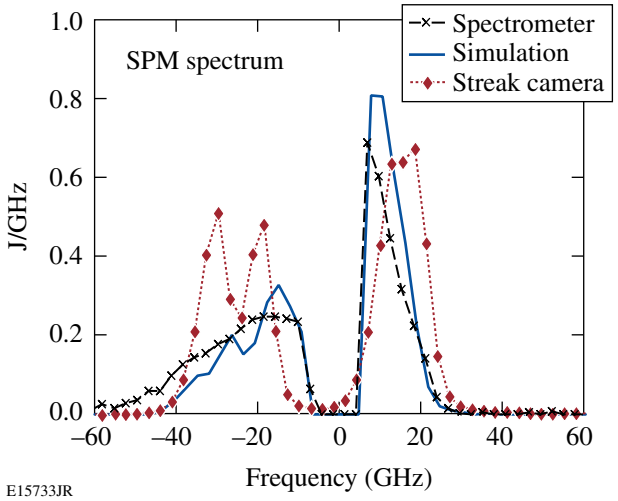

Figure 124.19
A comparison of the frequency-shifted spectra derived from the spectrometer (black curve with ×) with that derived from dP/dt as measured by the streak camera (red curve with diamonds) and predicted by the system model (solid blue curve). Frequencies within the resolution bandwidth of the spectrometer have been removed to highlight the shifted frequencies.

There is even better agreement between the model-generated spectrum and the measured spectrum. To achieve this agreement, the measured IR pulse shape at the input of the system had to be deconvolved with the 20-ps impulse response of the streak camera used to measure the pulse shape. This deconvolved pulse shape was applied to the laser system model to generate the predicted spectrum. The fact that deconvolution was necessary to match the measured spectrum indicates the high sensitivity of the spectroscopic measurement.

The IR and UV streak cameras and the UV spectrometer have been permanently installed on the system and are monitored on every shot. To further verify the model, a UV streak camera coupled to a spectrometer was temporarily installed to measure the time-resolved spectrum of the UV beam.[13] The centroid of the UV spectrum increases by approximately 0.2 Å from the nominal 3510.1 Å on the rising edge and decreases by 0.1 Å on the falling edge. The UV power history had a double Gaussian shape with a faster rising edge and slower falling edge as indicated by the dotted red curve in Fig. 124.20. The experimentally measured spectral shifts (black ×'s) closely

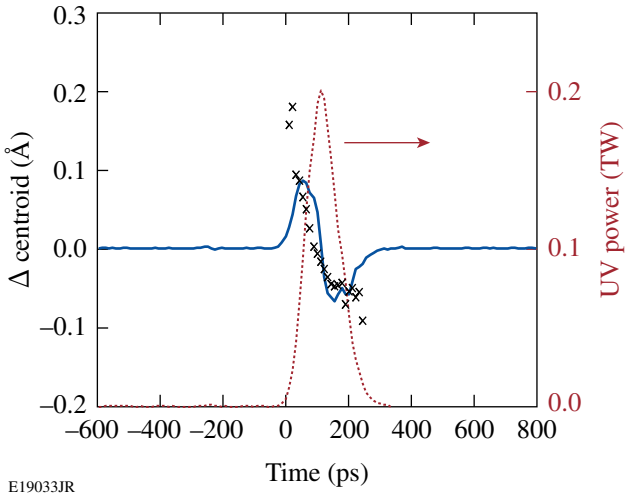

Figure 124.20
The time-resolved centroid of the UV spectrum (black ×'s) matches the derivative of the UV scaled by the constant 32 Å ps/TW (solid blue curve). The UV temporal shape is overlaid in red (dotted)

match the scaled temporal derivative of the UV power (solid blue curve). This verifies the temporal associations assumed in compiling Fig. 124.18.

These measurements help ensure the safety of the laser system. A scenario for safe operation of the laser system would be as follows: The IR pulse shape is measured at the input of the system, and the instrument temporal response is deconvolved to produce a high-bandwidth estimate of the input shape. This input pulse shape is processed by the model to determine if the pulse shape can be safely propagated through the system. The laser system is then fired and the spectrum is acquired. The measured SPM spectrum can then be converted into a ΣB-integral number to verify the pre-shot prediction.

Conclusion

We have, for the first time, demonstrated the ability to directly monitor the contribution of SPM to the spectrum at the output on a multikilojoule laser system. We have also demonstrated for the first time, to our knowledge, a direct measurement of the important laser parameter ΣB. This provides a real-time diagnostic that can be used to ensure safe operation of the system. This is particularly important as more-complex pulse shapes employing multiple pickets (i.e., 100-ps pulses preceding longer shaped pulses)[14] are deployed on the system.

ACKNOWLEDGMENT

This work was supported by the U.S. Department of Energy Office of Inertial Confinement Fusion under Cooperative Agreement No. DE-FC52-08NA28302, the University of Rochester, and the New York State Energy Research and Development Authority. The support of DOE does not constitute an endorsement by DOE of the views expressed in this article.

REFERENCES

1. D. C. Brown, in *High-Peak-Power Nd:Glass Laser Systems*, edited by D. L. MacAdam, Springer Series in Optical Sciences (Springer-Verlag, New York, 1981), Vol. 25, Chap. 7, Sec. 7.4, p. 214.
2. Common usage of the term "B"-integral: ΔB is always the B-integral accumulated between laser stages, usually defined as pinhole-to-pinhole. ΔB determines the damage threat from small-spatial-scale self-focusing and should never exceed 2 rad. ΣB refers to the total B-integral through the entire laser system from oscillator to target. It usually is a determining factor for the focal-spot size. It regulates the growth of the highest-frequency ripple that can make it through all of the pinholes. When used alone, B can refer to either ΔB or ΣB and is used when no distinction is necessary.
3. L. M. Frantz and J. S. Nodvik, J. Appl. Phys. **34**, 2346 (1963).
4. Y. R. Shen, *The Principles of Nonlinear Optics* (Wiley, New York, 1984), p. 242.
5. P. V. Avizonis and R. L. Grotbeck, J. Appl. Phys. **37**, 687 (1966).
6. C. Bibeau, "Evaluation of the $^4I_{11/2}$ Terminal Level Lifetime for Several Neodymium-Doped Laser Crystals and Glasses," Ph.D. thesis, Lawrence Livermore National Laboratory, 1995.
7. S. M. Yarema and D. Milam, IEEE J. Quantum Electron. **QE-18**, 1941 (1982).
8. R. S. Craxton, IEEE J. Quantum Electron. **QE-17**, 1771 (1981).
9. J. Trenholme *et al*., Shiva Nova CP&D Interim Report, Laser Fusion Program, Lawrence Livermore National Laboratory, Misc. 107, 2-3-2-324 (1977).
10. J. R. Marciante, W. R. Donaldson, and R. G. Roides, IEEE Photonics Technol. Lett. **19**, 1344 (2007).
11. W. R. Donaldson, R. Boni, R. L. Keck, and P. A. Jaanimagi, Rev. Sci. Instrum. **73**, 2606 (2002).
12. W. R. Donaldson, M. Millecchia, and R. Keck, Rev. Sci. Instrum. **76**, 073106 (2005).
13. S. P. Regan, D. K. Bradley, A. V. Chirokikh, R. S. Craxton, D. D. Meyerhofer, W. Seka, R. W. Short, A. Simon, R. P. J. Town, B. Yaakobi, J. J. Carroll III, and R. P. Drake, Phys. Plasmas **6**, 2072 (1999).
14. V. A. Smalyuk, V. N. Goncharov, K. S. Anderson, R. Betti, R. S. Craxton, J. A. Delettrez, D. D. Meyerhofer, S. P. Regan, and T. C. Sangster, Phys. Plasmas **14**, 032702 (2007).